Chinese Journal of Structural Chemistry 45 (2026) 100763

Contents lists available at ScienceDirect

Chinese Journal of Structural Chemistry

journal homepage: www.journals.elsevier.com/chinese-journal-of-structural-chemistry

Article

# $Ag(Te_2O_3)(PO_4)$: The first Ag-containing phosphate-tellurite nonlinear optical crystal featuring novel zigzag layered structure

Piao Tang[a,b], Xin Wen[a,c], Jindong Chen[a], Ning Ye[a], Guang Peng[a,*]

[a] State Key Laboratory of Crystal Materials, Tianjin Key Laboratory of Functional Crystal Materials, Institute of Functional Crystal, Tianjin University of Technology, Tianjin, 300384, China

[b] School of Metallurgy and Environment, Central South University, Changsha, 410083, China

[c] State Key Laboratory of Crystal Materials and Institute of Crystal Materials, Shandong University, Jinan, 250100, China

ARTICLE INFO

*Keywords:*
Nonlinear optical
Phosphate-tellurite
Second-harmonic generation
Functional group composite

ABSTRACT

Based on a functional group composite strategy, the first Ag-containing phosphate-tellurite nonlinear optical (NLO) crystal, $Ag(Te_2O_3)(PO_4)$, was synthesized *via* a subcritical hydrothermal method. This crystal crystallizes in the noncentrosymmetric space group $Pmn2_1$, featuring a unique zigzag two-dimensional $[(Te_2O_3)(PO_4)]_\infty$ layer. It possesses the strongest powder second-harmonic generation (SHG) response among all reported phosphate-tellurite compounds, reaching 2.1 × $KH_2PO_4$, along with a moderate birefringence of 0.045@546 nm. Theoretical calculations indicate that the $TeO_4$ group with stereochemically active lone-pair electrons, together with $AgO_7$ polyhedra and $PO_4$ group, synergistically contributes to its optical properties. This functional group composite strategy not only facilitates the integration of phosphate and tellurite units with $Ag^+$ cations, but also offers a versatile route for designing NLO materials across diverse inorganic systems.

Nonlinear optical (NLO) materials play a crucial role in solid-state lasers, enabling the generation of tunable laser outputs *via* their frequency conversion properties, which are widely used across various fields such as medical equipment, optical communications, sensors, optical storage, and high-precision devices [1–4]. Metal oxides are commonly employed in the development of NLO crystals operating across the deep-ultraviolet (DUV, < 200 nm), ultraviolet-visible-near infrared (UV-Vis-NIR), and even mid-infrared (2.5–5 μm) regions [5]. In these bands, a high-performance second-order NLO crystal typically requires to meet the following conditions: 1) a non-centrosymmetric (NCS) structure; 2) a wide transparency range with the largest possible bandgap ($E_g$), which is usually beneficial for achieving a high laser damage threshold; 3) a large second-harmonic generation (SHG) coefficient ($KH_2PO_4$ (KDP) with $d_{36} = 0.39$ p.m. $V^{-1}$ is usually used as a reference); 4) a sufficient birefringence ($\Delta n$) for optimal phase matching capability; 5) good crystal growth habit; 6) stable physical and chemical properties [6,7]. However, crystals that can meet all these conditions simultaneously are very rare. Although many excellent NLO crystals have been developed, the rapid advancement of laser technology keeps the development of novel NLO crystals a focal point and an active frontier in materials science.

The rapid development of NLO crystals has benefited from the proposal of anionic group theory, which states that the macroscopic NLO properties of crystals originate from the geometric superposition of microscopic functional units [8]. It implies that the selection of microscopic functional groups and the control of their spatial arrangement are crucial for obtaining ideal NLO crystals. Currently, commercially available NLO crystals mainly include $\beta$-$BaB_2O_4$ ($\beta$-BBO), $LiB_3O_5$ (LBO), $CsLiB_6O_{10}$ (CLBO), $BiB_3O_6$ (BIBO), KDP, $KTiOPO_4$ (KTP), $LiNbO_3$ (LN), *etc*. [9–15]. Such crystals are predominantly derived from borates, phosphates, and certain transition-metal oxides, because these compound systems can offer a remarkably rich structural diversity for the exploration of NLO crystals. Particularly, in borates and phosphates [4,16,17], the triangular $\pi$-conjugated $BO_3$ and tetrahedral $BO_4$ and $PO_4$ are widely recognized as two types of the most classic microscopic functional groups for NLO crystals, which can assemble into rich and diverse structures through flexible connection modes. In addition, their compounds often exhibit favorable physicochemical properties. Based on these two types of functional groups, a series of outstanding NLO crystals have been found in carbonates, nitrates, guanidine salts, cyanurates, sulfates, fluorooxoborates, fluorophosphate, polar tetrahedral organic molecular crystals, and so on through the isomorphic functional

This article is part of a special issue entitled: Structural Chemistry published in Chinese Journal of Structural Chemistry.

* Corresponding author.
*E-mail address:* gpeng@email.tjut.edu.cn (G. Peng).

https://doi.org/10.1016/j.cjsc.2025.100763
Received 15 August 2025; Received in revised form 24 September 2025; Accepted 6 October 2025
Available online 10 October 2025

group substitution ($CO_3$, $NO_3$, $C(NH_2)_3$, $C_3N_3O_3$, and $SO_4$) and local group modification (*e.g.*, $BO_3F$, $PO_3F$, $SO_3F$, $NH_2SO_3$, $SO_2(NH_2)_2$) strategies [18–46].

In recent years, mixing two types of NLO-active groups into a single crystal has emerged as an effective strategy for designing new NLO materials [3,47–59]. Moreover, the properties of crystals can be precisely tuned through the combination of functional groups with distinct characteristics. For example, introducing transition-metal oxide/fluorine octahedra (*e.g.*, $NbO_xF_{6-x}$, $VO_xF_{6-x}$, and $MoO_xF_{6-x}$) capable of generating Jahn-Teller distortions, or incorporating groups (*e.g.*, $IO_3$, $TeO_3$, and $TeO_4$) and cations with stereochemically active lone pairs (SCALP) (*e.g.*, $Pb^{2+}$ and $Bi^{3+}$), can significantly enhance the SHG response of crystals [60–67].

In our previous studies, a variety of crystals were synthesized *via* the functional group composite strategy, including the first metal borate-iodate NLO crystal $Be_2(BO_3)(IO_3)$ [68], the niobium-tellurite $LiNbTeO_5$ [69], the germanate-niobate $K_3Nb_3Ge_2O_{13}$ [70], the mercury-based tellurite-nitrates $Hg_3(TeO_3)_2(NO_3)_2$ and $Hg_3(Te_2O_5)_2(NO_3)_2$ [71], as well as the guanidinium sulfamate $[C_2N_4H_7O][NH_2SO_3]$ [72], *etc*. In this work, we further applied the same strategy to explore the phosphate-tellurite system and successfully incorporated the $d^{10}$ transition metal cation $Ag^+$, leading to the synthesis of the first Ag-containing phosphate-tellurite, $Ag(Te_2O_3)(PO_4)$. It should be noted that the reported phosphate-tellurites are scarce, which may be attributable to the synthetic difficulties. As a new member of the phosphate-tellurite family, the titled compound features a unique zigzag two-dimensional (2D) layered structure and exhibits the strongest SHG response of 2.1 × KDP, along with a moderate birefringence of 0.045@546 nm.

Single crystals of $Ag(Te_2O_3)(PO_4)$ were prepared by the subcritical hydrothermal method (see details in the Supporting Information (SI)). The phase purity was confirmed by powder XRD diffraction (Fig. S1(a)), and energy-dispersive X-ray spectroscopy (EDS) analysis confirmed the existence of Te, P, Ag, and O (Fig. S1(b)). Besides, bond valence calculations gave valence states of +1.0 for $Ag^+$, +3.79 for $Te^{4+}$, and +4.84 for $P^{5+}$, which agree well with their ideal values. Detailed crystallographic data and structural refinement parameters are listed in Table S1–4 of the SI.

$Ag(Te_2O_3)(PO_4)$ crystallizes in the NCS orthorhombic space group $Pmn2_1$ (No. 31) with cell parameters $a = 8.7625(6)$, $b = 7.3886(7)$, $c = 4.7013(3)$ Å and $Z = 2$. The asymmetric unit is composed of one P atom, one Te atom, one Ag atom, and five O atoms. All the Te atoms are connected to four O atoms to form seesaw $TeO_4$ groups with Te–O bond length ranges from 1.897(6) to 2.077(7) Å. The Ag atom coordinates with seven O atoms to form the $AgO_7$ polyhedron, and the bond length of Ag–O varies from 2.41(2) to 2.94(7) Å. All the P atoms are coordinated by four O atoms to form $PO_4$ groups with the P–O bonds in 1.526(9)–1.565(6) Å. As shown in Fig. 1(a), $Ag(Te_2O_3)(PO_4)$ features a 2D layered structure, in which $PO_4$ and $TeO_4$ groups interconnect through corner-sharing oxygen atoms, forming a zigzag $[(Te_2O_3)(PO_4)]_\infty$ 2D layer. The $Ag^+$ are located between the layers to balance the charge. Viewed along the *b*-axis, the $TeO_4$ groups are connected by sharing O atoms, forming 2D layers with 12-membered rings (MRs), within which the $PO_4$ groups are located (Fig. 1(b)). The calculated dipole moment of an individual $TeO_4$ is 15 Debye. The net dipole moment of all $TeO_4$ groups is enhanced by superposition along the *c*-axis. As Fig. 1(c) plots, the lone pair electrons on all $TeO_4$ units in this structure tend to point in the positive direction of the *c*-axis with an angle of ±38°, and such arrangement is favorable for enhancing the SHG effect.

Thermogravimetry-differential thermal analysis of $Ag(Te_2O_3)(PO_4)$ was performed in an argon atmosphere over the temperature range of 30–1200 °C. As shown in Fig. S2(a), a slight weight loss of ~1.6% observed at 360 °C is attributed to the cracking and fly-off of crystals during the heating process. An obvious endothermic peak appears at 548 °C without weight loss. The drastic weight loss occurring above 758 °C can be ascribed to the decomposition of $TeO_2$.

The UV-Vis-NIR diffuse reflectance spectrum of $Ag(Te_2O_3)(PO_4)$ powder samples was characterized (Fig. 2(a)). Its UV absorption cutoff edge is located at 274 nm. The corresponding band gap is 3.98 eV based on the transformation of the Kubelka-Munk function. As the infrared (IR) spectrum (Fig. S2(b)) of $Ag(Te_2O_3(PO_4)$ shows, the asymmetric and symmetric stretching vibrations of the $PO_4$ group were observed at 915–990 and 1096 $cm^{-1}$. Absorption peaks in the range of 418–627 $cm^{-1}$ were attributed to the vibrations of Te–O bonds. These values match well with other compounds containing P–O and Te–O functional groups.

The powder SHG effect of $Ag(Te_2O_3)(PO_4)$ was evaluated using the Kurtz-Perry method with a Q-switched Nd:YAG solid-state laser [73]. As shown in Fig. 2(b), the sample within the particle size range of 150–212 μm exhibits an SHG intensity of 2.1 × KDP@1064 nm. The SHG signal increases with particle size, indicating that $Ag(Te_2O_3)(PO_4)$ is phase-matchable.

To better understand the microscopic mechanism of the interaction between optical properties and electronic structures, the first-principles calculations were performed based on the density functional theory (DFT) [74–77]. As shown in Fig. S3, the top of the valence band (VB) and the bottom of the conduction band (CB) are located at different positions in *k*-space, indicating that $Ag(Te_2O_3)(PO_4)$ is an indirect bandgap

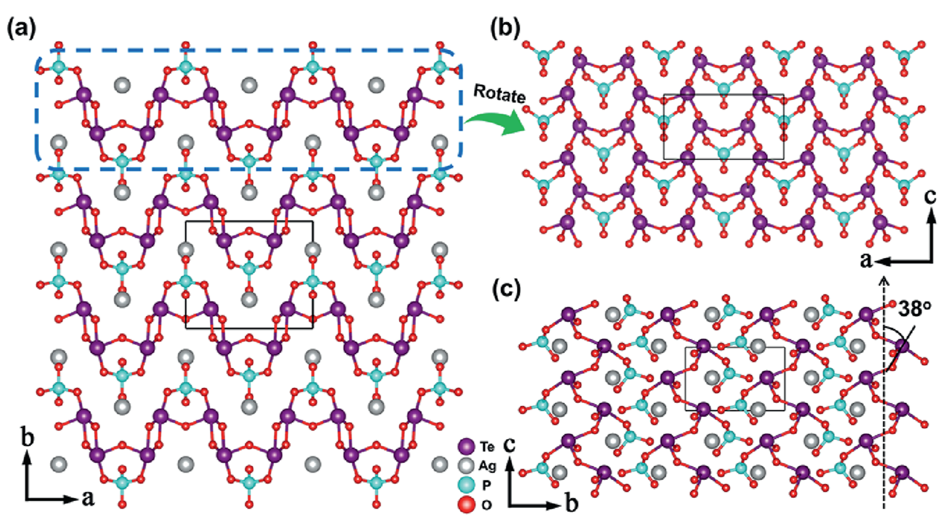


**Fig. 1.** Crystal structure of $Ag(Te_2O_3)(PO_4)$. (a) The layered structure of $Ag(Te_2O_3)(PO_4)$ viewed along the *c*-axis; (b) The $[(Te_2O_3)(PO_4)]_\infty$ layer viewed along the *b*-axis; (c) The structure of $Ag(Te_2O_3)(PO_4)$ viewed along the *a*-axis with the arrangement orientation of $TeO_4$ marked out.

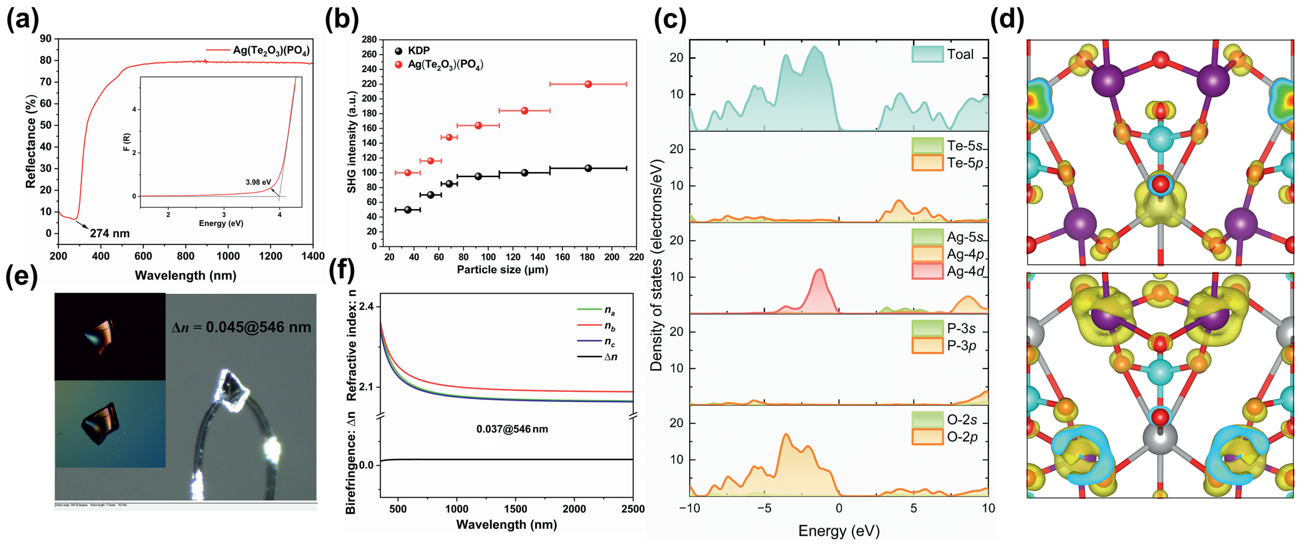


**Fig. 2.** Properties of $Ag(Te_2O_3)(PO_4)$. (a) The UV-Vis-NIR diffuse reflectance spectrum of $Ag(Te_2O_3)(PO_4)$; (b) The powder SHG measurements of $Ag(Te_2O_3)(PO_4)$ and KDP at 1064 nm; (c) Calculated total and partial DOS for $Ag(Te_2O_3)(PO_4)$; (d) SHG-weighted electron density maps of the occupied and unoccupied states in the VE process; (e) Crystal with interference colour for measuring the birefringence; (f) Calculated refractive index and birefringence for $Ag(Te_2O_3)(PO_4)$.

compound. Due to the discontinuity of the generalized gradient approximation (GGA) and the Perdew-Burke-Ernzerhof (PBE) functional, the theoretical bandgap was underestimated as 2.849 eV, compared to the experimental value of 3.98 eV [78]. Therefore, a scissors operation with a value of 1.041 eV was applied to adjust all conduction bands upwards to be consistent with experimental values [79]. Under the restriction of Kleinman symmetry, $Ag(Te_2O_3)(PO_4)$ has three independent nonzero SHG coefficients $d_{15}$, $d_{24}$, and $d_{33}$, which are calculated as 0.437, 1.206, and 0.760 p.m. $V^{-1}$ (Fig. S3(b)). Among them, $d_{24}$ is the largest tensor, which is approximately 3.1 × KDP.

Because the optical properties hinge on the electronic transitions near the Fermi level, we calculated the total density of states (DOS) and partial density of states (PDOS) for each element in $Ag(Te_2O_3)(PO_4)$. As shown in Fig. 2(c), the top of VB (−3–0 eV) is mainly occupied by O-2*p* and Ag-4*d* orbitals. In this region, Te-5*p* and P-3*p* orbitals made a minor contribution. As for the bottom of CB (0–5 eV), it is mainly occupied by Te-5*p* and O-2*p*. Both Ag-5*s* and P-3*p* orbitals made small contributions. It can be concluded that the optical properties of $Ag(Te_2O_3)(PO_4)$ are mainly determined by the $TeO_4$ groups. Meanwhile, $AgO_7$ polyhedra made non-negligible contributions, and the contribution of $PO_4$ is the least. Given that the SHG-weighted electron densities of occupied and unoccupied states in the virtual electron (VE) process predominantly govern the SHG response, the largest tensor $d_{24}$ was analyzed to intuitively elucidate the origin of the SHG effect. The result (Fig. 2(d)) further confirmed that the synergistic effect of $TeO_4$, $PO_4$, and $AgO_7$ polyhedra leads to the SHG effect of the crystal.

To determine the birefringence ($\Delta n$), a randomly oriented plate-like crystal of $Ag(Te_2O_3)(PO_4)$ with a thickness $d = 16.5$ μm was analyzed using a polarizing microscope equipped with a 546 nm monochromatic light source (Fig. 2(e)). The optical path difference $R$ was measured to be 750 nm. Based on the relationship $R = \Delta n \times d$, the birefringence of the selected $Ag(Te_2O_3)(PO_4)$ crystal was determined to be $\Delta n = 0.045$@546 nm. The calculated refractive index dispersion curve of $Ag(Te_2O_3)(PO_4)$ is shown in Fig. 2(f) with the order of refractive indices being $n_b > n_a > n_c$, and the birefringence being 0.037@546 nm, which is quite close to the experimental result. Additionally, $Ag(Te_2O_3)(PO_4)$ has been identified as a biaxial crystal.

Based on data from the Inorganic Crystal Structure Database (ICSD), a total of 14 phosphate-tellurites have been reported to date, of which 9 are centrosymmetric. The remaining 5 compounds are NCS but exhibit only very weak SHG responses, rarely exceeding 0.2 × KDP. As summarized in Table 1, $Ag(Te_2O_3)(PO_4)$ achieves a remarkably high SHG response of 2.1 × KDP, which represents the current record for this material system. It also possesses a comparably short UV cutoff edge (274 nm) and a large band gap (3.98 eV). However, its birefringence (0.045@546 nm) is the smallest among these compounds with available

**Table 1**
Optical properties of some phosphate-tellurites.

| Compound | Space group | Absorption edge (nm) | Band gap (eV) | SHG efficiency | Birefringence | Reference |
|---|---|---|---|---|---|---|
| $K_2TeP_2O_8$ | $P2_12_12$ | \ | 4.6 | < 0.1 × KDP | > 0.05@546 nm | [80] |
| $NaTePO_5$ | $P\bar{1}$ | \ | 3.83 | \ | 0.212@1064 nm | [81] |
| $SrTeP_2O_8$ | $P2_1/c$ | \ | 4.09 | \ | 0.133@1064 nm | [81] |
| $Ba_2TeP_2O_9$ | $P\bar{1}$ | \ | 4.28 | \ | 0.126@1064 nm | [81] |
| $K_2(TeO)P_2O_7$ | $P2_1$ | 299 | 4.16 | 0.1 × KDP | 0.07@1064 nm | [82] |
| $Rb_2(TeO)P_2O_7$ | $P2_12_12$ | 292 | 4.26 | 0.1 × KDP | 0.09@1064 nm | [82] |
| $Cs_2(TeO)P_2O_7$ | *Pnma* | 317 | 3.92 | \ | 0.06@1064 nm | [82] |
| $Cd_3(PO_4)(TePO_6)$ | $P2_1/c$ | \ | 3.52 | \ | 0.075@1064 nm | [83] |
| $Na_3Ca_4(TeO_3)(PO_4)_3$ | $P6_3$ | \ | 3.6 | 0.2 × KDP | 0.05@1064 nm | [84] |
| $Sr_2Zn_3Te_2P_2O_{14}$ | $P2_1/c$ | 275 | \ | \ | \ | [85] |
| $Pb_2Zn_3Te_2P_2O_{14}$ | $P2_1/c$ | 330 | \ | \ | \ | [85] |
| $Ba_2Zn_2TeP_2O_{11}$ | $P2_1/c$ | 278 | \ | \ | \ | [85] |
| $Te_2O(PO_4)_2$ | *Cc* | \ | 4 | 50 × $\alpha$-$SiO_2$ | \ | [86] |
| $\beta$-$Te_3O_3(PO_4)_2$ | $P2_1/n$ | 248 | 4.04 | \ | \ | [87] |
| $Ag(Te_2O_3)(PO_4)$ | $Pmn2_1$ | 274 | 3.98 | 2.1 × KDP | Cal. 0.037@546 nm<br>Exp. 0.045@546 nm | This work |

data. This indirectly indicates that compounds in this class generally exhibit relatively large birefringence.

In conclusion, based on the functional group composite strategy, the first Ag-containing phosphate-tellurite NLO material, $Ag(Te_2O_3)(PO_4)$, has been successfully synthesized via the subcritical hydrothermal method. This crystal exhibits an excellent powder SHG effect ($2.1 \times$ KDP) and a moderate birefringence (0.045@546 nm). Theoretical calculations demonstrate that the synergistic effect of $TeO_4$, $AgO_7$, and $PO_4$ was responsible for the SHG effect. This work not only provides a promising NLO candidate crystal but also offers new references for exploring new phosphate-tellurite NLO materials.

## CRediT authorship contribution statement

**Piao Tang:** Writing – original draft, Investigation, Formal analysis, Data curation. **Xin Wen:** Validation, Software, Methodology. **Jindong Chen:** Funding acquisition, Formal analysis. **Ning Ye:** Funding acquisition, Formal analysis. **Guang Peng:** Writing – review & editing, Funding acquisition, Conceptualization.

## Declaration of competing interest

The authors declare no competing interests.

## Acknowledgements

We acknowledge the financial support by the National Natural Science Foundation of China (22375147, 52332001, 22305174), the National Key Research and Development Plan of the Ministry of Science and Technology (2023YFF0718900), and the Natural Science Foundation of Tianjin City (22JCYBJC01380).

## Appendix A. Supplementary data

Supplementary data to this article can be found online at https://doi.org/10.1016/j.cjsc.2025.100763.

Supporting Information is available free of charge via the Internet at http://pubs.acs.org.

Experimental details, tables of detailed crystallographic data and structure refinements, IR curves, and TG curve (PDF). The X-ray crystallographic file for the CCDC number is 2479486 (CIF).

## References

[1] R.A. Kumar, Borate crystals for nonlinear optical and laser applications: a review, J. Chem. 2013 (2013) 154862.
[2] T.T. Tran, H. Yu, J.M. Rondinelli, K.R. Poeppelmeier, P.S. Halasyamani, Deep ultraviolet nonlinear optical materials, Chem. Mater. 28 (2016) 5238–5258.
[3] Y. Pan, S.P. Guo, B.W. Liu, H.G. Xue, G.C. Guo, Second-order nonlinear optical crystals with mixed anions, Coord. Chem. Rev. 374 (2018) 464–496.
[4] M. Mutailipu, K.R. Poeppelmeier, S. Pan, Borates: a rich source for optical materials, Chem. Rev. 121 (2020) 1130–1202.
[5] K.M. Ok, Toward the rational design of novel noncentrosymmetric materials: factors influencing the framework structures, Acc. Chem. Res. 49 (2016) 2774–2785.
[6] P.S. Halasyamani, J.M. Rondinelli, The must-have and nice-to-have experimental and computational requirements for functional frequency doubling deep-UV crystals, Nat. Commun. 9 (2018) 2972.
[7] W.J. Yao, R. He, X.Y. Wang, Z.S. Lin, C.T. Chen, Analysis of deep-UV nonlinear optical borates: approaching the end, Adv. Opt. Mater. 2 (2014) 411–417.
[8] C.T. Chen, Y.C. Wu, R.K. Li, The anionic group theory of the non-linear optical effect and its applications in the development of new high-quality NLO crystals in the borate series, Int. Rev. Phys. Chem. 8 (1989) 65–91.
[9] C.C. Chen, B.C. Wu, A.D. Jiang, G.M. You, A new-type ultraviolet SHG crystal—$\beta$-$BaB_2O_4$, Sci. China Chem. 28 (1985) 235–243.
[10] C.T. Chen, Y.C. Wu, A.D. Jiang, B.C. Wu, G.M. You, R.K. Li, S.J. Lin, New nonlinear-optical crystal: $LiB_3O_5$, J. Opt. Soc. Am. B 6 (1989) 616–621.
[11] J.M. Tu, D.A. Keszler, $CsLiB_6O_{10}$: a noncentrosymmetric polyborate, Mater. Res. Bull. 30 (1995) 209–215.
[12] H. Hellwig, J. Liebertz, L. Bohaý, Exceptional large nonlinear optical coefficients in the monoclinic bismuth borate $BiB_3O_6$, Solid State Commun. 109 (1999) 249–251.
[13] J.J. De Yoreo, A.K. Burnham, P.K. Whitman, Developing $KH_2PO_4$ and $KD_2PO_4$ crystals for the world's most power laser, Int. Mater. Rev. 47 (2002) 113–152.
[14] A.H. Reshak, I.V. Kityk, S. Auluck, Investigation of the linear and nonlinear optical susceptibilities of $KTiOPO_4$ single crystals: theory and experiment, J. Phys. Chem. B 114 (2010) 16705–16712.
[15] A.A. Ballman, Growth of Piezoelectric and Ferroelectric Materials by the CzochraIski Technique, vol. 48, 1965, pp. 112–113.
[16] J. Chen, L. Xiong, L. Chen, L.M. Wu, $Ba_2NaClP_2O_7$: unprecedented phase matchability induced by symmetry breaking and its unique fresnoite-type structure, J. Am. Chem. Soc. 140 (2018) 14082–14086.
[17] G.S. Xu, X. Bai, Z.H. Yang, J. Han, S.L. Pan, $\pi$-Conjugated cations in phosphates: a pathway to solar-blind UV nonlinear optical crystals with phase-matching, Angew. Chem. Int. 64 (2025) e202510363.
[18] G.H. Zou, N. Ye, L. Huang, X.S. Lin, Alkaline-alkaline earth fluoride carbonate crystals $ABCO_3F$ (A = K, Rb, Cs; B = Ca, Sr, Ba) as nonlinear optical materials, J. Am. Chem. Soc. 133 (2011) 20001–20007.
[19] T.T. Tran, J. He, J.M. Rondinelli, P.S. Halasyamani, $RbMgCO_3F$: a new beryllium-free deep-ultraviolet nonlinear optical material, J. Am. Chem. Soc. 137 (2015) 10504–10507.
[20] Y.C. Liu, Y.G. Shen, S.G. Zhao, J.H. Luo, Structure-property relationship in nonlinear optical materials with $\pi$-conjugated $CO_3$ triangles, Coord. Chem. Rev. 407 (2020) 213152.
[21] G. Peng, C.S. Lin, N. Ye, $NaZnCO_3(OH)$: a high-performance carbonate ultraviolet nonlinear optical crystal derived from $KBe_2BO_3F_2$, J. Am. Chem. Soc. 142 (2020) 20542–20546.
[22] X.M. Liu, L. Kang, P.F. Gong, Z.S. Lin, $LiZn(OH)CO_3$: a deep-ultraviolet nonlinear optical hydroxycarbonate designed from a diamond-like structure, Angew. Chem. Int. Ed. 60 (2021) 13574–13578.
[23] X.M. Liu, P.F. Gong, Y. Yang, G.M. Song, Z.S. Lin, Nitrate nonlinear optical crystals: a survey on structure-performance relationships, Coord. Chem. Rev. 400 (2019) 213045.
[24] M. Luo, C.S. Lin, D.H. Lin, N. Ye, Rational design of the metal-free $KBe_2BO_3F_2\cdot$(KBBF) family member $C(NH_2)_3SO_3F$ with ultraviolet optical nonlinearity, Angew. Chem. Int. Ed. 59 (2020) 15978–15981.
[25] C. Wu, X.X. Jiang, Z.J. Wang, H.Y. Sha, Z.S. Lin, Z.P. Huang, X.F. Long, M. G. Humphrey, C. Zhang, UV solar-blind-region phase-matchable optical nonlinearity and anisotropy in a $\pi$-conjugated cation-containing phosphate, Angew. Chem. Int. Ed. 60 (2021) 14806–14810.
[26] M. Mutailipu, J. Han, Z. Li, F.M. Li, J.J. Li, F.F. Zhang, X.F. Long, Z.H. Yang, S. L. Pan, Achieving the full-wavelength phase-matching for efficient nonlinear optical frequency conversion in $C(NH_2)_3BF_4$, Nat. Photonics 17 (2023) 694–701.
[27] D.H. Lin, M. Luo, C.S. Lin, F. Xu, N. Ye, $KLi(HC_3N_3O_3)\cdot 2H_2O$: solvent-drop grinding method toward the hydro-isocyanurate nonlinear optical crystal, J. Am. Chem. Soc. 141 (2019) 3390–3394.
[28] X. Meng, W. Yin, M. Xia, Cyanurates consisting of intrinsic planar $\pi$-conjugated 6-membered rings: an emerging source of optical functional materials, Coord. Chem. Rev. 439 (2021) 213916.
[29] X.H. Meng, X.Y. Zhang, Q.X. Liu, Z.Y. Zhou, X.X. Jiang, Y.G. Wang, Z.S. Lin, M. J. Xia, Perfectly encoding $\pi$-conjugated anions in the $RE_5(C_3N_3O_3)(OH)_{12}$ (RE = Y, Yb, Lu) family with strong second harmonic generation response and balanced birefringence, Angew. Chem. Int. Ed. 62 (2023) e202214848.
[30] X.H. Dong, L. Huang, C.F. Hu, H.M. Zeng, Z.E. Lin, X. Wang, K.M. Ok, G.H. Zou, $CsSbF_2SO_4$: an excellent ultraviolet nonlinear optical sulfate with a $KTiOPO_4$ (KTP)-type structure, Angew. Chem. Int. Ed. 58 (2019) 6528–6534.
[31] Y.Q. Li, F. Liang, S.G. Zhao, L.N. Li, Z.Y. Wu, Q.R. Ding, S. Liu, Z.S. Lin, M.C. Hong, J.H. Luo, Two non-$\pi$-conjugated deep-UV nonlinear optical sulfates, J. Am. Chem. Soc. 141 (2019) 3833–3837.
[32] Y.Q. Li, C.L. Yin, X.Y. Yang, X.J. Kuang, J. Chen, L.H. He, Q.R. Ding, S.G. Zhao, M. C. Hong, J.H. Luo, A nonlinear optical switchable sulfate of ultrawide bandgap, CCS Chem. 3 (2021) 2298–2306.
[33] C. Wu, X.X. Jiang, Y.L. Hu, C.B. Jiang, T.H. Wu, Z.S. Lin, Z.P. Huang, M. G. Humphrey, C. Zhang, A lanthanum ammonium sulfate double salt with a strong SHG response and wide deep-UV transparency, Angew. Chem. Int. Ed. 61 (2022) e202115855.
[34] C. Wu, T.H. Wu, X.X. Jiang, Z.J. Wang, H.Y. Sha, L. Lin, Z.S. Lin, Z.P. Huang, X. F. Long, M.G. Humphrey, C. Zhang, Large second-harmonic response and giant birefringence of $CeF_2(SO_4)$ induced by highly polarizable polyhedra, J. Am. Chem. Soc. 143 (2021) 4138–4142.
[35] Y.C. Yang, X. Liu, J. Lu, L.M. Wu, L. Chen, $[Ag(NH_3)_2]_2SO_4$: a strategy for the coordination of cationic moieties to design nonlinear optical materials, Angew. Chem. Int. Ed. 60 (2021) 21216–21220.
[36] X.H. Dong, L. Huang, H.M. Zeng, Z.E. Lin, K.M. Ok, G.H. Zou, High-performance sulfate optical materials exhibiting giant second harmonic generation and large birefringence, Angew. Chem. Int. Ed. 61 (2022) e202116790.
[37] Z.Y. Bai, K.M. Ok, Designing sulfate crystals with strong optical anisotropy through $\pi$-conjugated tailoring, Angew. Chem. Int. Ed. 63 (2024) e202315311.
[38] C. Wu, C.B. Jiang, G.F. Wei, X.X. Jiang, Z.J. Wang, Z.S. Lin, Z.P. Huang, M. G. Humphrey, C. Zhang, Toward large second-harmonic generation and deep-UV transparency in strongly electropositive transition metal sulfates, J. Am. Chem. Soc. 145 (2023) 3040–3046.
[39] G.Q. Shi, Y. Wang, F.F. Zhang, B.B. Zhang, Z.H. Yang, X.L. Hou, S.L. Pan, K. R. Poeppelmeier, Finding the next deep-ultraviolet nonlinear optical material: $NH_4B_4O_6F$, J. Am. Chem. Soc. 139 (2017) 10645–10648.
[40] M. Mutailipu, M. Zhang, Z.H. Yang, S.L. Pan, Targeting the next generation of deep-ultraviolet nonlinear optical materials: expanding from borates to borate fluorides to fluorooxoborates, Acc. Chem. Res. 52 (2019) 791–801.

[41] C.C. Jin, F.M. Li, B.L. Cheng, H.T. Qiu, Z.H. Yang, S.L. Pan, M. Mutailipu, Double-modification oriented design of a deep-UV birefringent crystal functionalized by $[B_{12}O_{16}F_4(OH)_4]$ clusters, Angew. Chem. Int. Ed. 61 (2022) e202203984.

[42] J. Lu, J.N. Yue, L. Xiong, W.K. Zhang, L. Chen, L.M. Wu, Uniform alignment of non-π-conjugated species enhances deep ultraviolet optical nonlinearity, J. Am. Chem. Soc. 141 (2019) 8093–8097.

[43] X. Hao, M. Luo, C.S. Lin, G. Peng, F. Xu, N. Ye, $M(NH_2SO_3)_2$ (M = Sr, Ba): two deep-ultraviolet transparent sulfamates exhibiting strong second harmonic generation responses and moderate birefringence, Angew. Chem. Int. Ed. 60 (2021) 7621–7625.

[44] W.Q. Huang, S.G. Zhao, J.H. Luo, Recent development of non-π-conjugated deep ultraviolet nonlinear optical materials, Chem. Mater. 34 (2021) 5–28.

[45] H.T. Tian, N. Ye, M. Luo, Sulfamide: a promising deep-ultraviolet nonlinear optical crystal assembled from polar covalent $[SO_2(NH_2)_2]$ tetrahedra, Angew. Chem. Int. Ed. 61 (2022) e202200395.

[46] Y.G. Chen, X.X. Jiang, H.X. Lv, D.J. Mei, X. Zhang, Y. Guo, Z.S. Lin, X.M. Zhang, Two $\alpha$-$SiO_2$-related deep-ultraviolet phase-matchable optical nonlinear beryllium silicate crystals $Na_2BeSiO_4$ and $Li_2BeSiO_4$ with enhanced SHG effect, Small 21 (2025) 2408360.

[47] J.L. Song, C.L. Hu, X. Xu, F. Kong, J.G. Mao, A facile synthetic route to a new SHG material with two types of parallel π-conjugated planar triangular units, Angew. Chem. Int. Ed. 54 (2015) 3679–3682.

[48] M.J. Xia, X.X. Jiang, Z.S. Lin, R.K. Li, "All-three-in-one": a new bismuth-tellurium-borate $Bi_3TeBO_9$ exhibiting strong second harmonic generation response, J. Am. Chem. Soc. 138 (2016) 14190–14193.

[49] J. Chen, C.L. Hu, F.F. Mao, J.H. Feng, J.G. Mao, A facile route to nonlinear optical materials: three-site aliovalent substitution involving one cation and two anions, Angew. Chem. Int. Ed. 58 (2019) 2098–2102.

[50] J. Chen, C.L. Hu, X.H. Zhang, B.X. Li, B.P. Yang, J.G. Mao, $CsVO_2F(IO_3)$: an excellent SHG material featuring an unprecedented 3D $[VO_2F(IO_3)]^-$ anionic framework, Angew. Chem. Int. Ed. 59 (2020) 5381–5384.

[51] Q.R. Ding, X.M. Liu, S.G. Zhao, Y.S. Wang, Y.Q. Li, L. Li, S. Liu, Z.S. Lin, M.C. Hong, J.H. Luo, Designing a deep-UV nonlinear optical fluorooxosilicophosphate, J. Am. Chem. Soc. 142 (2020) 6472–6476.

[52] C. Wu, X.X. Jiang, Z.J. Wang, L. Lin, Z.S. Lin, Z.P. Huang, X.F. Long, M.G. Humphrey, C. Zhang, Giant optical anisotropy in the UV-transparent 2D nonlinear optical material $Sc(IO_3)_2(NO_3)$, Angew. Chem. Int. Ed. 60 (2021) 3464–3468.

[53] B.L. Cheng, Z.J. Li, Y. Chu, A. Tudi, M. Mutailipu, F.F. Zhang, Z.H. Yang, S.L. Pan, $(NH_4)_3B_{11}PO_{19}F_3$: a deep-UV nonlinear optical crystal with unique $[B_5PO_{10}F]_\infty$ layers, Natl. Sci. Rev. 9 (2022) nwac110.

[54] H.N. Liu, H.P. Wu, Z.G. Hu, J.Y. Wang, Y.C. Wu, H.W. Yu, $Cs_3[(BOP)_2(B_3O_7)_3]$: a deep-ultraviolet nonlinear optical crystal designed by optimizing matching of cation and anion groups, J. Am. Chem. Soc. 145 (2023) 12691–12700.

[55] D.Y. Dou, Q. Shi, H.M. Li, B.B. Zhang, D.Q. Yang, Y. Wang, Rational combination of π-conjugated and non-π-conjugated groups achieving strong nonlinear optical response, large optical anisotropy, and UV light-switchable fluorescence, Adv. Sci. 11 (2024) 2401325.

[56] Y.W. Kang, C. Yang, J. Gou, Y.L. Zhu, Q.W. Zhu, W.L. Xu, Q. Wu, From Cd $(SCN)_2(CH_4N_2S)_2$ to $Cd(SCN)_2(C_4H_6N_2)_2$: controlling sulfur content in thiocyanate systems significantly improves the overall performance of UV nonlinear optical materials, Angew. Chem. Int. Ed. 63 (2024) e202402086.

[57] Z.P. Zhang, X. Liu, R.X. Wang, S. Zhao, W.J. He, H.Y. Chen, X.B. Deng, L.M. Wu, Z. Zhou, L. Chen, Remarkable second harmonic generation response in $(C_5H_6NO)^+(CH_3SO_3)^-$: unraveling the role of hydrogen bond in thermal driven nonlinear optical switch, Angew. Chem. Int. Ed. 63 (2024) e202408551.

[58] Y.L. Deng, C.L. Hu, X. Xu, M.Z. Zhang, J.G. Mao, $Na[B_3IO_7(OH)]$ and $Na_2[B_4IO_9](IO_3)$: explorations of boroiodates with strong second harmonic generation response and large birefringence, J. Am. Chem. Soc. 147 (2025) 12858–12865.

[59] D.Z. Lu, Y.Z. Wang, X.H. Li, F. Liang, K. Wu, H.H. Yu, H.J. Zhang, $La_3ZrGa_5O_{14}$: band-inversion strategy in topology-protected octahedron for large nonlinear response and wide bandgap, Angew. Chem. Int. Ed. 64 (2025) e202503341.

[60] J. Chen, C.L. Hu, Y.L. Li, Q.Q. Chen, B.X. Li, J.G. Mao, $AMoO_3(IO_3)$ (A = Na and K): two promising optical materials via properly assembling the Λ-shaped basic building units, J. Alloys Compd. 894 (2022) 162547.

[61] Y. Hou, H.P. Wu, H.W. Yu, Z.G. Hu, J.Y. Wang, Y.C. Wu, An effective strategy for designing nonlinear optical crystals by combining the structure-directing property of oxyfluorides with chemical substitution, Angew. Chem. Int. Ed. 60 (2021) 25302–25306.

[62] H.X. Tang, Y.X. Zhang, C. Zhuo, R.B. Fu, H. Lin, Z.J. Ma, X.T. Wu, A niobium oxyiodate sulfate with a strong second-harmonic-generation response built by rational multi-component design, Angew. Chem. Int. Ed. 58 (2019) 3824–3828.

[63] X.L. Cao, C.L. Hu, X. Xu, F. Kong, J.G. Mao, $Pb_2TiOF(SeO_3)_2Cl$ and $Pb_2NbO_2(SeO_3)_2Cl$: small changes in structure induced a very large SHG enhancement, Chem. Commun. 49 (2013) 9965–9967.

[64] B.P. Yang, C.L. Hu, X. Xu, C. Huang, J.G. Mao, $Zn_2(VO_4)(IO_3)$: a novel polar zinc(II) vanadium(V) iodate with a large SHG response, Inorg. Chem. 52 (2013) 5378–5384.

[65] C. Wu, X.X. Jiang, Z.J. Wang, L. Lin, Z.S. Lin, Z.P. Huang, X.F. Long, M. G. Humphrey, C. Zhang, Giant optical anisotropy in the UV-transparent 2D nonlinear optical material $Sc(IO_3)_2(NO_3)$, Angew. Chem. Int. Ed. 60 (2021) 3464–3468.

[66] F. Kong, S.P. Huang, Z.M. Sun, J.G. Mao, W.D. Cheng, $Se_2(B_2O_7)$: a new type of second-order NLO material, J. Am. Chem. Soc. 128 (2006) 7750–7751.

[67] H.W. Yu, J. Cantwell, H.P. Wu, W.G. Zhang, K.R. Poeppelmeier, P.S. Halasyamani, Top-seeded solution crystal growth, morphology, optical and thermal properties of $Ba_3(ZnB_5O_{10})PO_4$, Cryst. Growth Des. 16 (2016) 3976–3982.

[68] G. Peng, C.S. Lin, H.X. Fan, K.C. Chen, B.X. Li, G. Zhang, N. Ye, $Be_2(BO_3)(IO_3)$: the first anion-mixed Van der Waals member in the $KBe_2BO_3F_2$ family with a very strong second harmonic generation response, Angew. Chem. Int. Ed. 60 (2021) 17415–17418.

[69] K.C. Chen, C.S. Lin, G. Peng, Y. Chen, H.Z. Huang, E.Z. Chen, Y.X. Min, T. Yan, M. Luo, N. Ye, $LiNbTeO_5$: a high-performance multifunctional crystal material with a very large second-harmonic generation response and piezoelectric coefficient, Chem. Mater. 34 (2022) 399–404.

[70] K.C. Chen, C.S. Lin, J.D. Chen, G.S. Yang, H.T. Tian, M. Luo, T. Yan, Z.G. Hu, J. Y. Wang, Y.C. Wu, N. Ye, G. Peng, Intense d-p hybridization in $Nb_3O_{15}$ tripolymer induced the largest second harmonic generation response and birefringence in germanates, Angew. Chem. Int. Ed. 62 (2023) e202217039.

[71] P. Tang, X. Wen, Y.C. Yan, X. Cao, J.D. Chen, C.S. Lin, M. Luo, N. Ye, G. Peng, $Hg_3(TeO_3)_2(NO_3)_2$ and $Hg_3(Te_2O_5)_2(NO_3)_2$: the first two Hg-based tellurite nitrate unit-mixed crystals with large optical anisotropy, Laser Photonics Rev. 9 (2025) 2500014.

[72] X. Wen, Y. Yan, J.Y. Lu, X.M. Shi, P. Tang, J.D. Chen, G.S. Yang, G. Peng, H.H. Yu, H.J. Zhang, Z.G. Hu, J.Y. Wang, N. Ye, $[C_2N_4H_7O][NH_2SO_3]$: high-performance ultraviolet nonlinear optical crystal with ditrigon coupled guanylurea group, Angew. Chem. Int. Ed. 64 (2025) e202424153.

[73] S.K. Kurtz, T.T. Perry, A powder technique for the evaluation of nonlinear optical materials, J. Appl. Phys. 39 (1968) 3798–3813.

[74] M.C. Payne, M.P. Teter, D.C. Allan, T.A. Arias, J.D. Joannopoulos, Iterative minimization techniques forab initiototal-energy calculations: molecular dynamics and conjugate gradients, Rev. Mod. Phys. 64 (1992) 1045–1097.

[75] S.J. Clark, M.D. Segall, C.J. Pickard, P.J. Hasnip, M.I.J. Probert, K. Refson, M. C. Payne, First principles methods using CASTEP, Z. Kristallogr. 220 (2005) 567–570.

[76] A.M. Rappe, K.M. Rabe, E. Kaxiras, J.D. Joannopoulos, Optimized pseudopotentials, Phys. Rev. B 41 (1990) 1227–1230.

[77] D.J. Moss, E. Ghahramani, J.E. Sipe, H.M. van Driel, Band-structure calculation of dispersion and anisotropy in χ→(3) for third-harmonic generation in Si, Ge, and GaAs, Phys. Rev. B 41 (1990) 1542–1560.

[78] J.P. Perdew, K. Burke, M. Ernzerhof, Generalized gradient approximation made simple, Phys. Rev. Lett. 77 (1996) 3865–3868.

[79] R.W. Godby, M. Schluter, L.J. Sham, Self-energy operators and exchange-correlation potentials in semiconductors, Phys. Rev. B 37 (1988) 10159–10175.

[80] M. Wen, C. Hu, Z.H. Yang, X.H. Wu, S.L. Pan, $K_2TeP_2O_8$: a new telluro-phosphate with a pentagonal Te–P–O layer structure, Dalton Trans. 47 (2018) 9453–9458.

[81] M. Zhao, Y.J. Sun, Y.D. Wu, D.J. Mei, S.G. Wen, T. Doert, $NaTePO_5$, $SrTeP_2O_8$ and $Ba_2TeP_2O_9$: three tellurite-phosphates with large birefringence, J. Alloys Compd. 854 (2021) 157243.

[82] M. Zhao, W.M. Dong, Y.D. Wu, D.J. Mei, S.G. Wen, T. Doert, $A_2(TeO)P_2O_7$ (A = K, Rb, Cs): three new tellurite-pyrophosphates with large birefringence, J. Alloys Compd. 865 (2021) 158785.

[83] W.D. Yao, M. Yan, X.H. Li, W.L. Liu, R.L. Tang, $Cd_3(PO_4)(TePO_6)$: a novel cadmium tellurite-phosphate featuring a $\{[TePO_6]^{3-}\}_\infty$ chain, Eur. J. Inorg. Chem. 2021 (2021) 4566–4571.

[84] Z. Li, S.Z. Zhang, W.L. Yin, Z.S. Lin, J.Y. Yao, Y.C. Wu, $Na_3Ca_4(TeO_3)(PO_4)_3$: a new noncentrosymmetric tellurite phosphate with fascinating multimember-ring architectures and intriguing nonlinear optical performance, Dalton Trans. 47 (2018) 17198–17201.

[85] M.J. Xia, R.K. Li, Structural variety in zinc telluro-phosphates: syntheses, crystal structures and characterizations of $Sr_2Zn_3Te_2P_2O_{14}$, $Pb_2Zn_3Te_2P_2O_{14}$ and $Ba_2Zn_2TeP_2O_{11}$, Dalton Trans. 45 (2016) 7492–7499.

[86] M.K. Kim, S.H. Kim, H.Y. Chang, P.S. Halasyamani, K.M. Ok, New noncentrosymmetric tellurite phosphate material: synthesis, characterization, and calculations of $Te_2O(PO_4)_2$, Inorg. Chem. 49 (2010) 7028–7034.

[87] L. Li, R.C. Zhuang, J.X. Mi, Y.X. Huang, A new modification of tellurite phosphate: $\beta$-$Te_3O_3(PO_4)_2$, Chin. J. Struct. Chem. 37 (2018) 1417–1425.